PNAS

www.pnas.org

Supplementary Information for

Characterization of superoligomeric DNA-protein complexes by nanoparticle tracking analysis and association with disease severity in in systemic lupus erythematosus

Kristian Juul-Madsen, Anne Troldborg, Thomas Wittenborn, Mads Axelsen, Huaying Zhao, Lasse Klausen, Stefanie Luecke, Søren Paludan, Kristian Stengaard-Pedersen, Mingdong Dong, Holger Møller, Steffen Thiel, Henrik Jensen, Peter Schuck, Duncan Sutherland, Søren Degn and Thomas Vorup-Jensen

Correspondence to: vorup-jensen@biomed.au.dk

This PDF file includes:

Figures S1 to S9
Tables S1
SI References
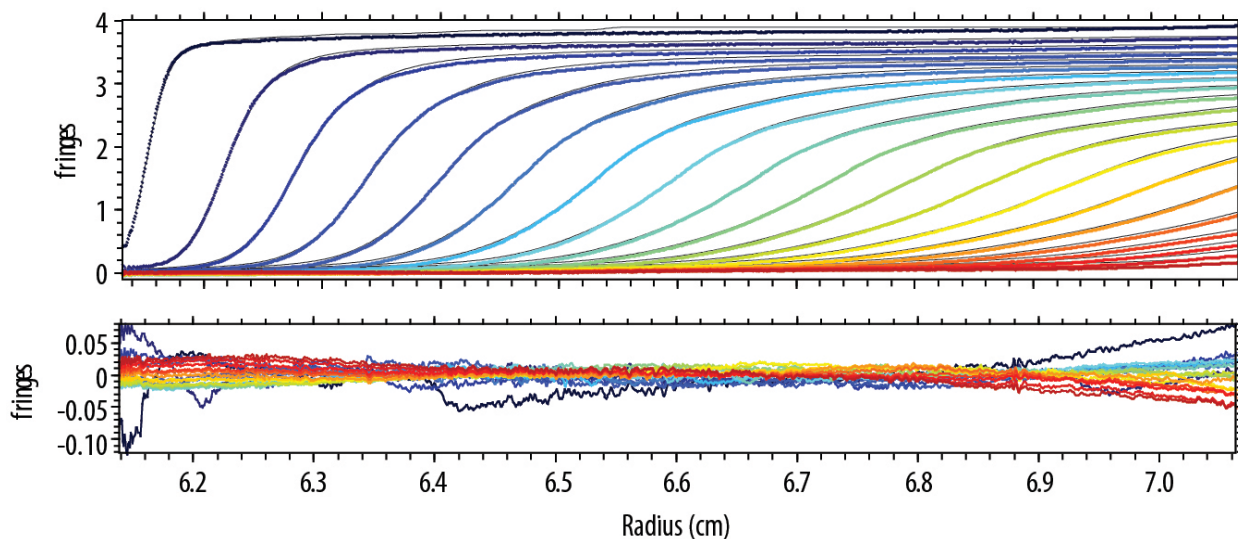
Fig. S1.

Rayleigh interference optical sedimentation boundaries of 1 mg/mL MBL in PBS, pH 7.4, sedimenting at 50,000 rpm (dotted lines) and best-fit from the *c(s)* model (solid black lines). Residuals are shown in the lower panel. The root-mean-square deviation is 0.003-fold the loading signal. Each scan is shown in a color temperature indicating the evolution of time.
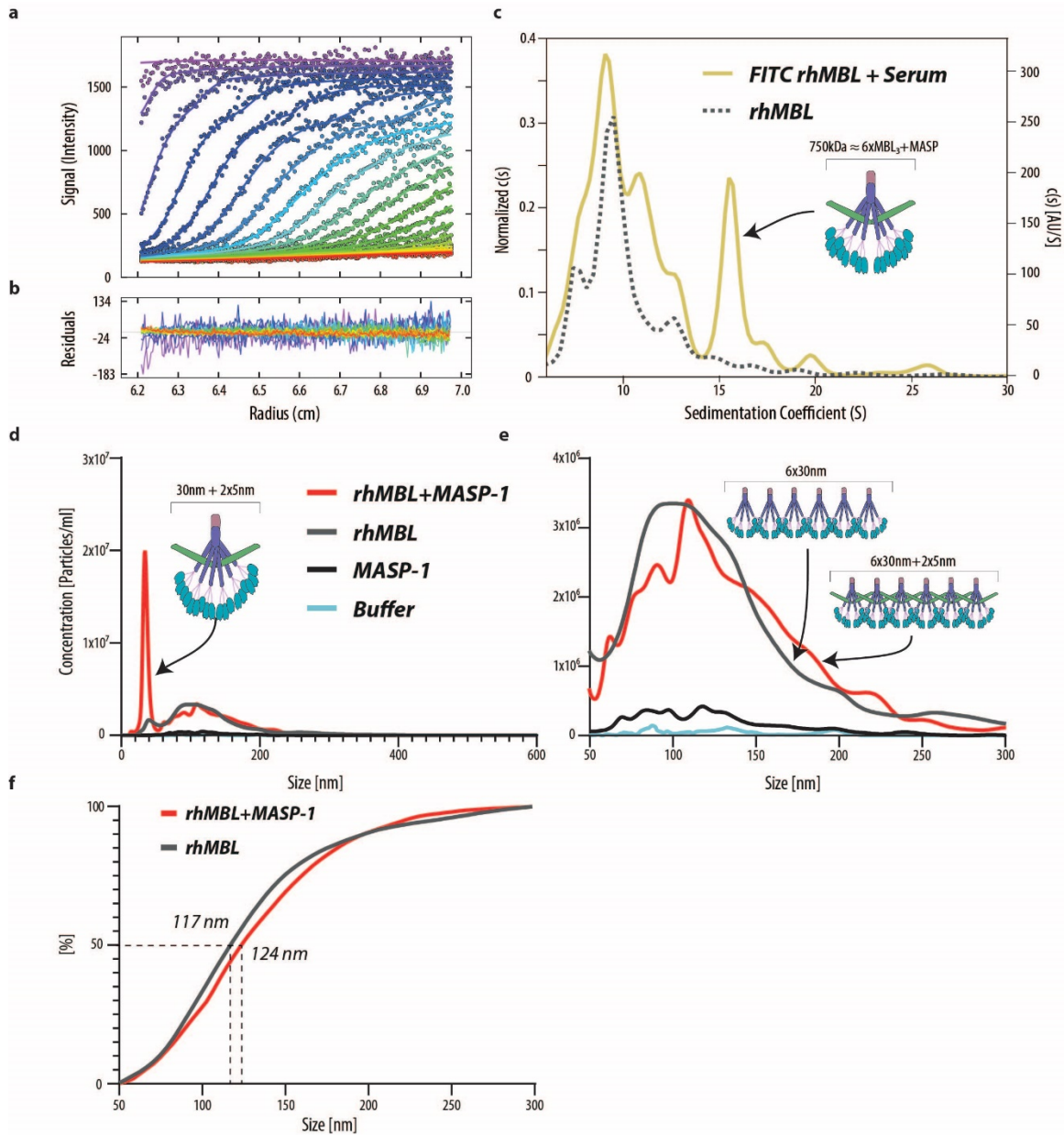
Fig. S2.

Fluorescence-detected SV of MBL-FITC in 10% (v/v) human serum, sedimenting at 50,000 rpm and 20 °C and association between rhMBL and MASP-1. (a) Data points (circles, for clarity reduced to every 2nd data point of every 2nd scan) and best-fit boundaries from the *c(s)* model (solid lines) for the centrifugation of MBL-FITC in serum. Residuals are shown in (b) as overlay. The root-mean-square deviation was 1.4% of the loading signal. Each scan is shown in a color temperature indicating the evolution of time. (c) The sedimentation coefficient distribution *c(s)* for the MBL-FITC experiment overlayed with the sedimentation profile for rhMBL at 1 mg/ml. A schematic model of the 6×MBL$_3$/MASP indicates the approximate sedimentation coefficient for this complex. (d-f) The association between rhMBL and MASP-1 was measured with NTA in 3 experiments based on light scattering, each with 5 technical replicates. (d) The mean size

3

distribution as a function of concentration in the interval from 0-600 nm. Addition of MASP-1 showed an increased population of particles above limit of detection at 40 nm corresponding to MASP-1 binding. (e) As a result of MASP-1 binding, protein particles in the interval from 50-300 nm showed a small increase in the size with a change in median size from 177 nm to 124 nm (f) comparable to the expected change in geometry of binding MASP-1 to superoligomeric MBL as indicated with schematics.
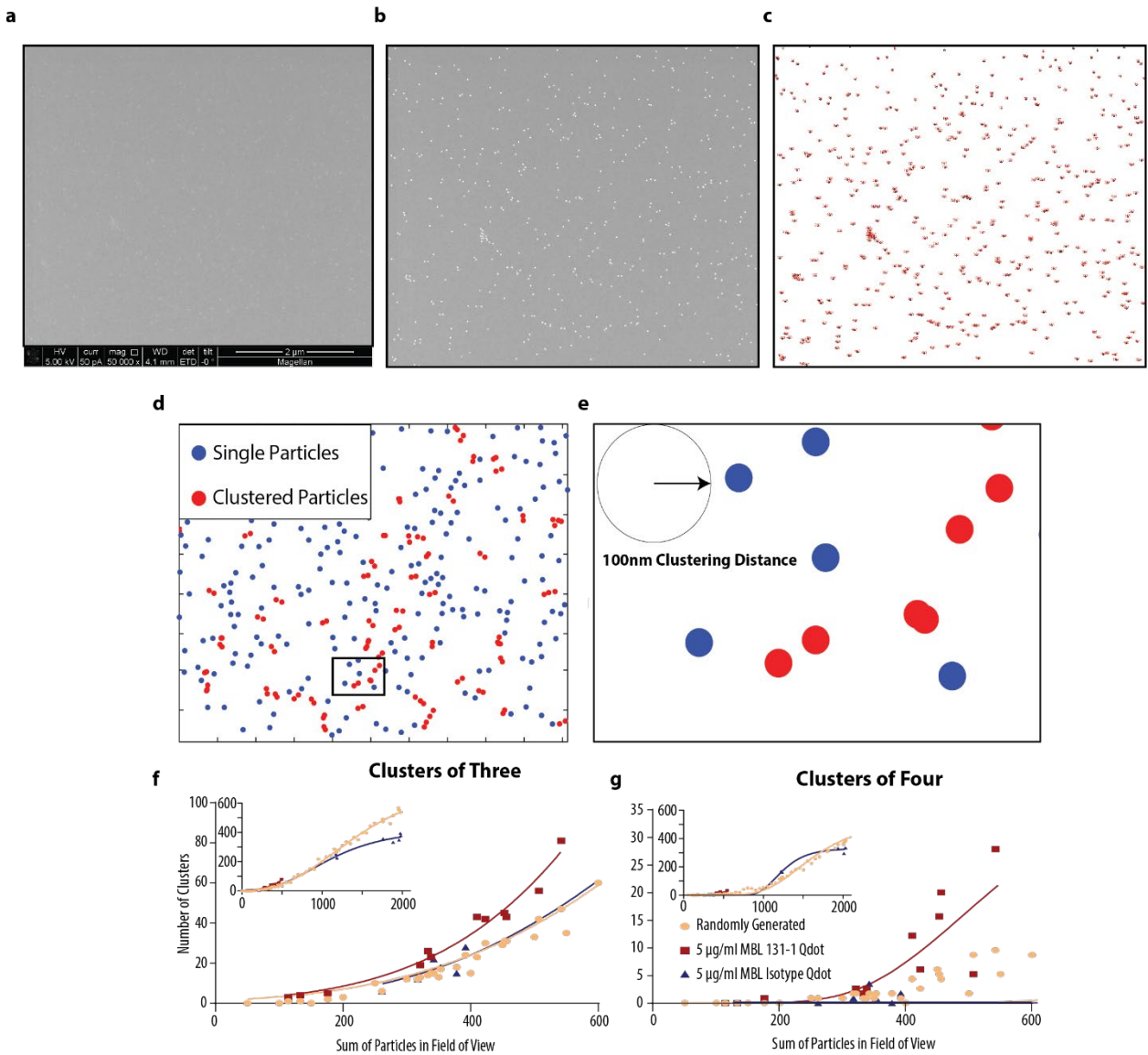
Fig. S3.

Clustering of Ab Q-dot conjugates is driven by MBL specificity. (a) Raw SEM image of a silicon wafer Ti PVD-coated surface treated with MBL 5 µg/mL for 30 min and incubated with anti MBL Ab QD. (b) Manual contrast enhancement of the raw image using ImageJ. (c) Counting and positioning of the particles using analyze particles function in ImageJ. (d-e) Nearest-neighbor distance analysis and cluster formation based on a maximum of 100 nm proximity from center to center to the nearest neighbor. (f-g) Cluster analysis of experimentally generated surfaces and simulated surfaces with random positioning of particles in an equal size field of view. Data was fitted to a Gompertz growth model using Graphpad Prism. (f) Analysis of clusters with three or more particles. (g) Analysis of clusters with four or more particles.
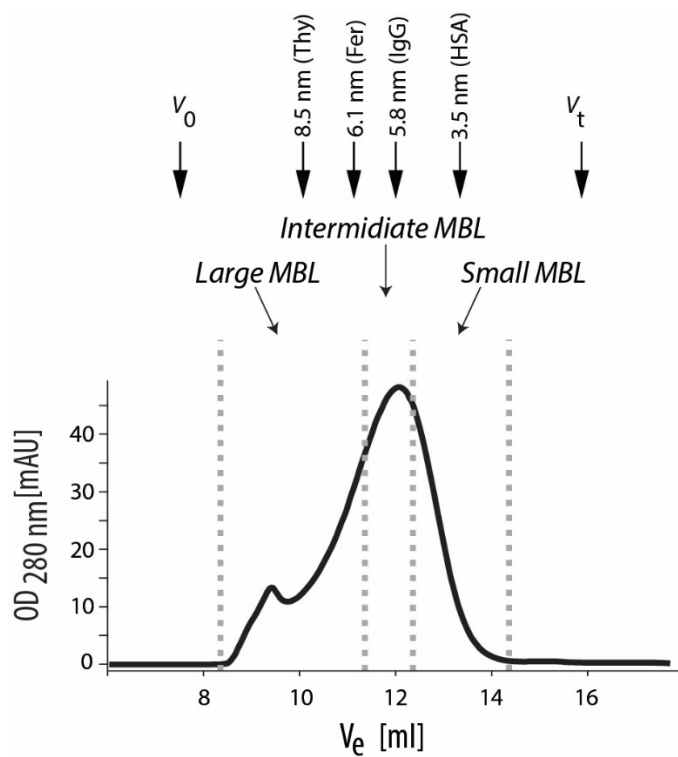
Fig. S4.
Separation of MBL into small, intermediate, and large oligomers by GPC. Void and elution volumes are indicated (V_0 and V_t respectively) as well as the elution of calibration molecules. Dashed gray lines indicate separation into large, medium and small sized MBL fractions. The shown elution profile is representative of 3 experiments.
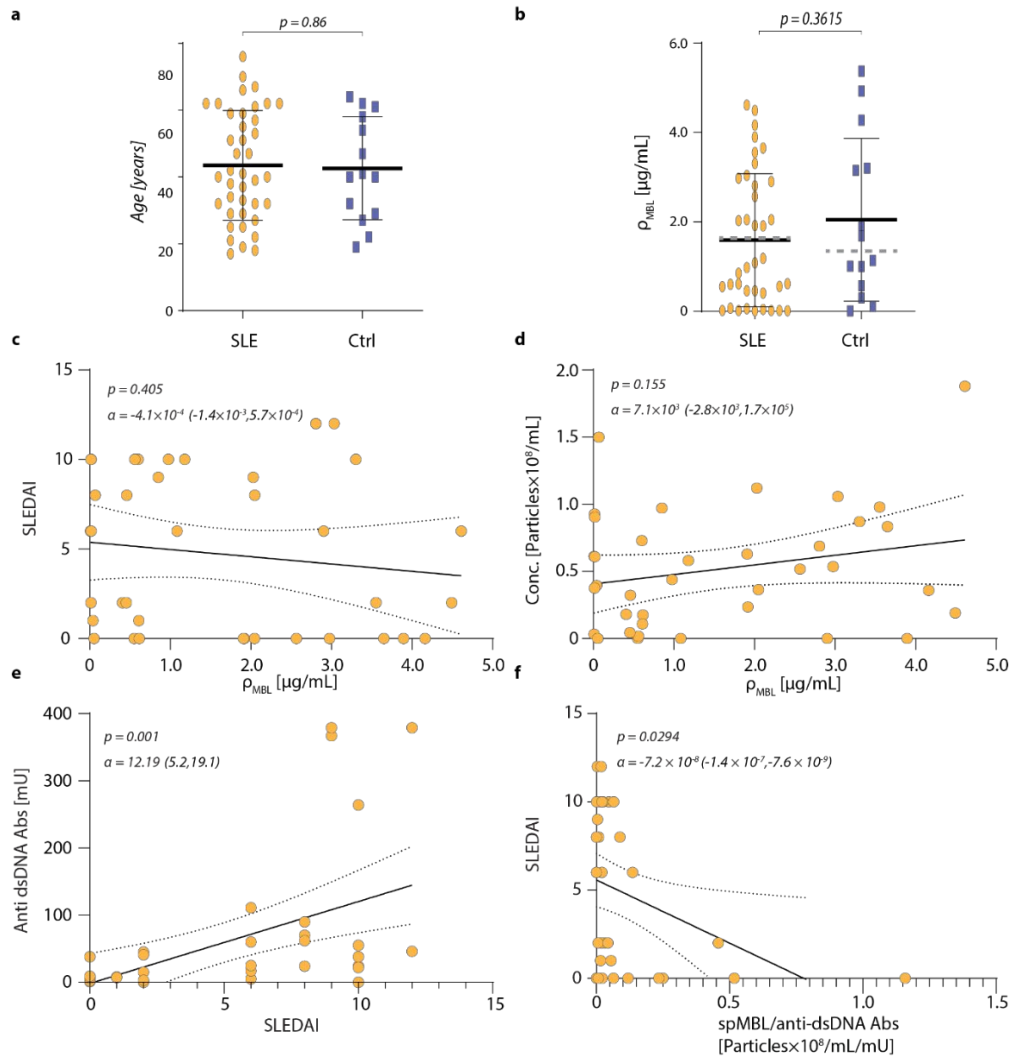
Fig. S5.

(a) Age-match between patients ($N = 39$) and HCs ($N = 14$) compared in a two-tailed t-test. Solid line and error bars indicate mean and SEM. (b) Concentration of MBL in HCs and SLE patients measured earlier by TRIFMA(1). Mean values were consistent with previously reported values for these cohorts (gray dashed lines). Data was analyzed with a two-tailed t-test with Welch's correction. (c) MBL total concentration measured by TRIFMA was not correlated with SLEDAI score. Data was analyzed with a linear regression model (solid black line) with and confidence intervals α (dotted lines). P-value signifies the likelihood of α being equal to zero. (d) The MBL concentration measured by TRIFMA was not correlated with the concentration of 200–300 nm MBL complexes measured with NTA. Data was analyzed as indicated in (c). Anti dsDNA Ab were positively correlated with SLEDAI. Data was analyzed as indicated in (c). (f) Linear regression was calculated according to the expression α·[spMBL]/[Anti-dsDNA Ab]+β and indicated with a solid line (confidence interval shown in dotted lines). p value states the likelihood of α =0. Concentration of spMBL and anti dsDNA Ab was negatively correlated with the SLEDAI score. Data was analyzed as indicated in (c).

a

b
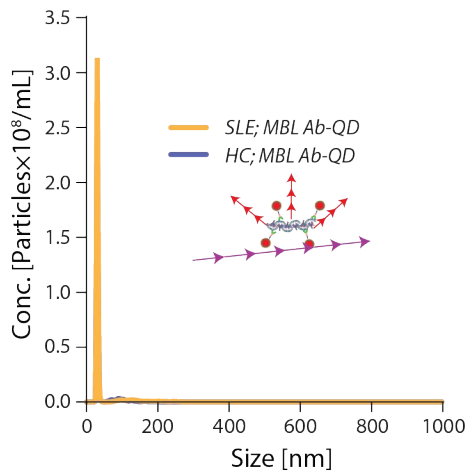
c
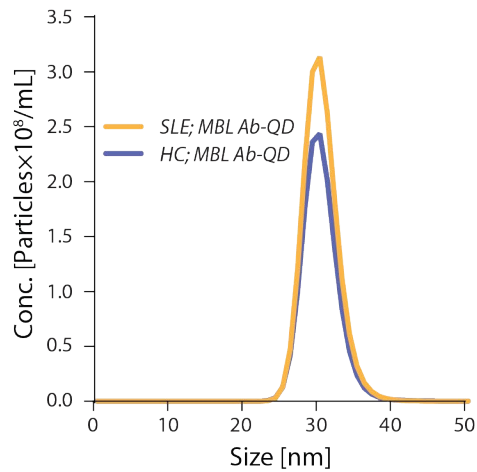
Fig. S6.

(a) Raw image from NTA recording of SLE patient plasma incubated with MBL Ab-QD reporters. Samples were dominated by smaller species with only a blurred outline and a small fraction of more distinct, larger structures. (b) Average concentration of particles detected in size range 0-1000 nm for SLE patients ($N = 39$) and HCs ($N = 14$). (c) Average concentration of particles detected in size range 0-50 nm for SLE patients ($N = 39$) and HCs ($N = 14$). Ab-QD conjugation is pure with a single peak at 30 nm.
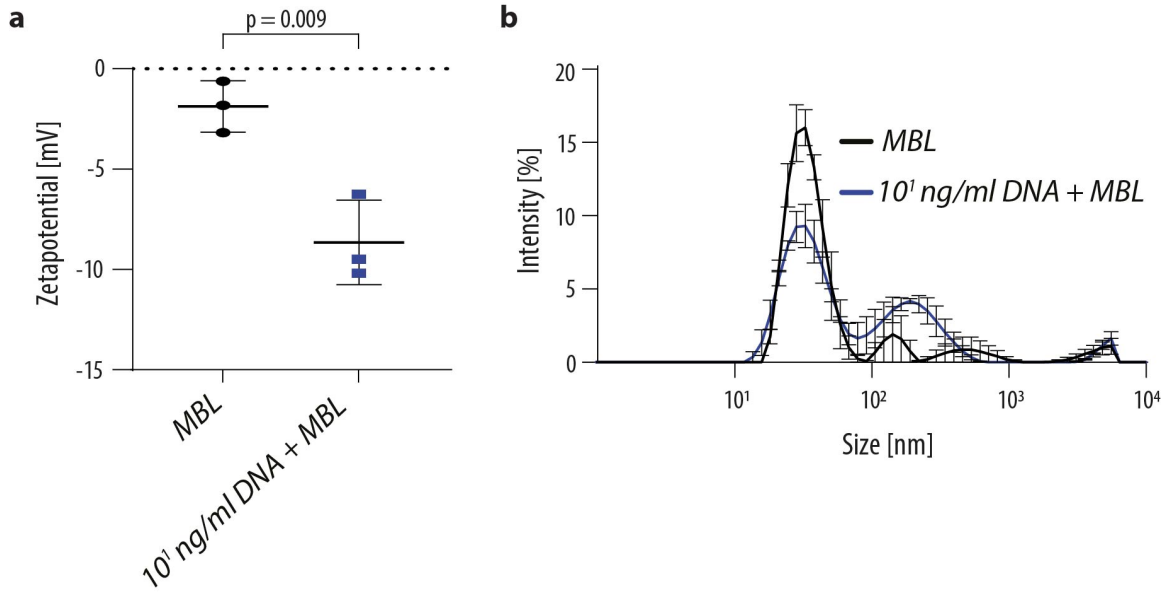
Fig. S7.

Determination of the zeta potential for MBL/DNA complexes. (a) The zeta potential was measured for MBL particles at 10 µg/ml or for MBL at 10 µg/ml with 10 ng/ml 4570bp dsDNA, with each condition measured in three experiments. Error bars indicate SD. An unpaired *t*-test assessed the difference in mean values with a p-value of 0.009. (b) The MBL particle size was estimated with dynamic light scattering for MBL at 10 µg/ml or at 10 µg/ml with 10 ng/ml 4570bp dsDNA. Curves show the mean values of 3 experiments and error bars show SD.

a
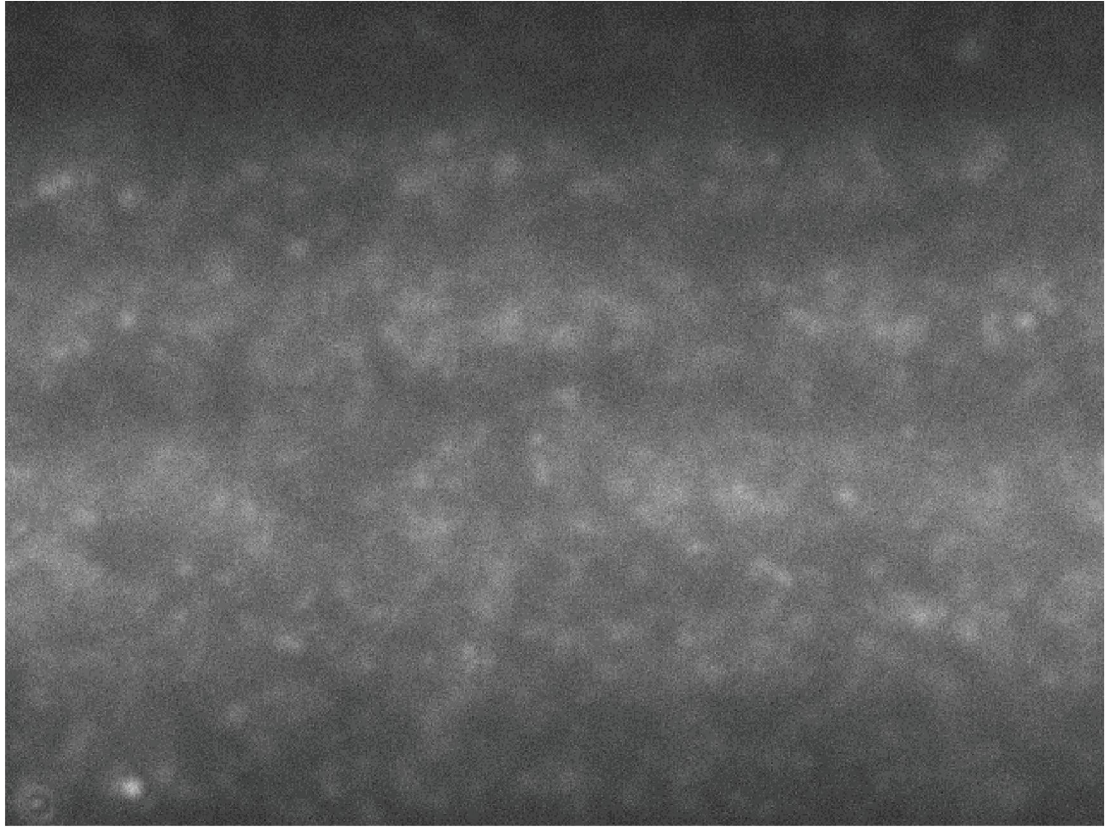
b
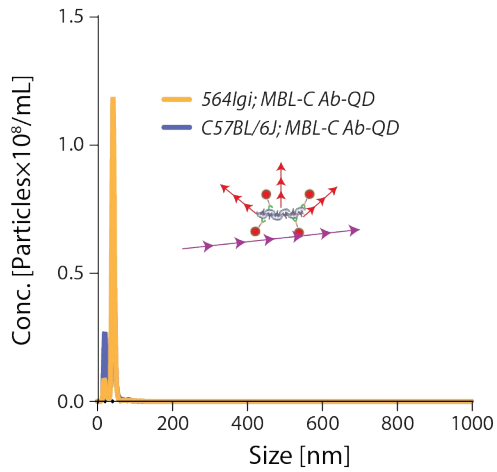
c
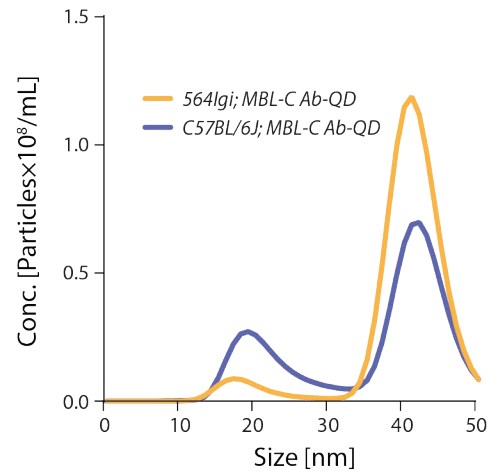
Fig. S8.

(a) Raw image from NTA recording of 564Igi plasma incubated with MBL-C Ab-QD reporters. (b) Average concentration of particles detected in size range 0-1000 nm for 564Igi mice ($N = 16$) and C57BL/6J mice ($N = 14$). (c) Average concentration of particles detected in size range 0-50 nm. Peak at 20nm show a small degree of unconjugated QDs.
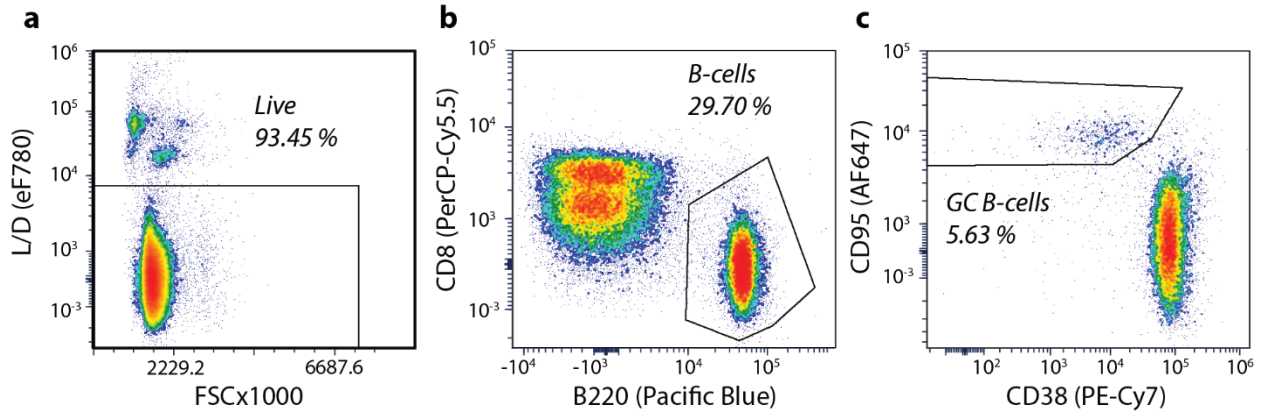
Fig. S9.

Gating strategy for quantification of GC B cells in splenocytes. Live cells (a) were gated for B220$^{\text{High}}$CD8$^{\text{Neg}}$B220^{+} B cells (b), which were further analyzed for the content of CD95^{+}CD38$^{\text{dim}}$ GC B cells (c). Representative gating for 564Igi mice are shown.

Patient number	39
Age at inclusion, mean (sd)	44.5 (16.8)
Age at diagnosis, mean (sd)	32.1 (14.6)
Gender F (%)	89.7
Ethnicity: Caucasian (%)	100

ACR criterias (cumulative)

Number of ACR criterias, mean (sd)	6.3 (1.1)
Malar rash (ACR1) (%)	69
Discoid lupus (ACR2) (%)	7.7
Photosensitivity (ACR3) (%)	64.1
Oral/nasal ulcers (ACR4) (%)	43.6
Arthritis (ACR5) (%)	89.7
Serositis (ACR6) (%)	41
Nephritis (ACR7) (%)	28.2
CNS (ACR8) (%)	7.7
Hematological (ACR9) (%)	74,4
Immunological (ACR10) (%)	94.9
ANA (ACR11) (%)	97.4

Clinical and biochemical data at time of inclusion

SLEDAI at inclusion, mean (sd)	4.8 (4.31)
SLICC, mean (sd)	1.1 (1.34)
Proteinurea > 0.5g/day (%)	15.4
Anti-phospholipid syndrome (%)	25.6

Treatment at time of inclusion

Hydroxychloroquine treatment (%)	79.5
Prednisolone treatment (%)	61.5
Other immuno-suppressants (%)*	41.0

Table S1.

Patient demographics. Patients were randomly chosen from a larger cohort of SLE patients described elsewhere (1). Only selection criteria from the larger patient cohort was to ensure an even spread between patients with a low SLEDAI score of 2 or below and patients with a high SLEDAI score of 6 or above. *Azathioprine, Mycophenolate, Methotrexat.*

SI References

1.   A. Troldborg *et al.*, The Lectin Pathway of Complement Activation in Patients with Systemic Lupus Erythematosus. *J Rheumatol* **45**, 1136-1144 (2018).